

Effect of ionic strength on PNA-DNA hybridization on surfaces and in solution

Hyeyoung Park

Max-Planck-Institute for Polymer Research, Ackermannweg 10, D-55128 Mainz, Germany

Andrea Germini, Stefano Sforza, Roberto Corradini, and Rosangela Marchelli

Department of Organic and Industrial Chemistry, University of Parma, Parco Area delle Scienze 17/A, 43100 Parma, Italy

Wolfgang Knoll^{a)}

Max-Planck-Institute for Polymer Research, Ackermannweg 10, D-55128 Mainz, Germany

(Received 29 January 2007; accepted 8 May 2007; published 19 June 2007)

Peptide nucleic acids (PNAs) are mimics of oligonucleotides containing a neutral peptidic backbone and are able to bind complementary DNA targets with high affinity and selectivity. In order to investigate the effect of the ionic strength of the buffer solution, hybridization experiments with PNAs as (catcher) probes and DNAs as target oligonucleotides were performed in different salt solutions. Surface plasmon field-enhanced fluorescence spectroscopy was employed for real-time monitoring of DNA hybridizations to surface bound PNA. Probes with three different strand lengths were immobilized by self-assembly on the sensor surface. By introducing Cy5-labeled DNA targets the affinity constants, $K_A = k_{\text{on}} / k_{\text{off}}$ (association/dissociation), were determined for fully complementary (MM0) as well as for single base mismatched (MM1) duplexes. Furthermore, the thermal stability of each duplex was determined by measuring melting curves in solution which was then compared to the kinetic and affinity parameters determined for the surface hybridization reactions. The results indicate that ions do not play a significant role for the PNA/DNA hybridization kinetics at surfaces. However, changes in the configuration of the PNA/DNA duplex due to the ionic strength variations influence the fluorescence yield drastically. © 2007 American Vacuum Society. [DOI: 10.1116/1.2746871]

I. INTRODUCTION

Biosensors are self-contained, integrated devices using a biological recognition element, which is in direct contact with the transduction module.¹ Such devices need to be rapid and simple and should have sufficient sensitivity and high selectivity for the detection of analyte molecules. This need is realized in optical evanescent wave biosensors²⁻⁷ which offer a versatile approach for the detection and characterization of biological molecules. The most commonly employed biosensors are surface plasmon resonance (SPR) biosensors⁸⁻¹⁴ with microfluidic sample handling. For hybridization studies and DNA detection, catcher molecules are immobilized to the sensor surface, and the binding process is monitored in real time after injection of a target analyte solution, detecting small local changes in refractive index at the sensor surface upon the biomolecular interaction. However, for the detection of short oligonucleotides having only several tens of base pairs and for catcher matrices of relatively low surface density, the small changes of the refractive index are not sufficient to quantitatively analyze the surface hybridization reaction in detail. Recently, surface plasmon field-enhanced fluorescence spectroscopy (SPFS), which is a combination of SPR and fluorescence detection, has been introduced.¹⁵ Upon the binding of chromophore-labeled targets to the catcher probes, the analyte molecules at the metal/

solution interface are within the evanescent field of the surface plasmon mode, thus allowing the chromophores to be excited giving rise to a significantly enhanced fluorescence intensity. In order to get a high fluorescence yield, the distance between the chromophores and the metal surface needs to be optimized by employing functional self-assembled architecture avoiding quenching effects.¹⁶⁻¹⁹ This fluorescence signal shows sufficient sensitivity to allow for the analysis of the rate constants of biomolecular interactions quantitatively even in the picomolar ($10^{-12}M$) concentration range of the target.²⁰ As the catcher probe layer, peptide nucleic acids (PNAs) as mimics of DNA show great potential for biosensor applications. Instead of the sugarphosphates of DNAs, PNAs have a neutral *N*-(2-aminoethyl) glycine backbone to which the nucleobases are attached.²¹ Several advantages have been demonstrated using PNA rather than DNA probes for sensor-based hybridization studies. Firstly, the hybrid stability expressed by the thermal stability (e.g., by the melting temperature T_m) of the PNA-DNA duplexes displays in general a higher value than the corresponding DNA-DNA duplexes at physiological ionic strength. Secondly, given the fact that PNA has a noncharged pseudopeptide backbone, its physicochemical properties differ significantly from polyanionic oligonucleotides.

DNA is a highly charged polyelectrolyte. The negative charges of the phosphates have to be neutralized by counterions, which may be metal ions, organic amines, positively

^{a)}Electronic mail: knoll@mpip-mainz.mpg.de

charged proteins or, in therapeutic applications, positively charged drugs²²⁻²⁸ Therefore, ionic strength has a major influence on the DNA/DNA duplex formation, while in solution it affects PNA/DNA duplex formation less extensively.²⁹ PNAs have been used in a variety of methods for diagnostics and gene analysis, both in solution and immobilized on solid surfaces.³⁰ The latter is becoming increasingly important in application such as microarray technology³¹ and SPR biosensors.³² For example, the detection of point mutations related to genetic diseases was accomplished using SPR technologies and PNAs (Ref. 33) or modified PNAs.³⁴ Therefore, the understanding of the effects which could be important in mismatch recognition on surfaces is useful in the rational design of new PNA-based sensors.

In this article, the hybridization reactions between PNAs and DNAs having three different lengths (11-mer, 13-mer, and 15-mer), both fully matched (MM0) or exhibiting one base mismatch (MM1), were analyzed quantitatively on the sensor surface and in solution. From the SPFS data, the rate constants for association (k_{on}) and dissociation (k_{off}) and the affinity constant (K_A) of the hybridization were determined by fitting the experimental data by a simple Langmuir model. Additionally, the thermodynamic parameters of the PNA/DNA duplexes were determined by Van't Hoff plots of the melting curves recorded in solution.

In order to evaluate the effect of the ionic strength on the behavior of PNA probes on the sensor surface, hybridization reactions of MM0 and MM1 PNA/DNA duplexes were studied in buffer solutions of high (NaCl=137 mM) and low (NaCl=20 mM) ionic strengths, respectively. Additionally, the limit of the ionic strength for PNA/DNA hybridization was investigated at different concentrations of phosphate buffer (without adding salt) and in pure water.

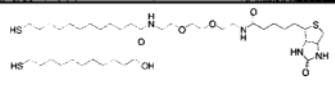

II. EXPERIMENTAL SECTION

A. Materials

All DNA oligonucleotides (purity >98.5% as checked by high performance liquid chromatography, HPLC) were purchased from MWG-Biotech AG. Full match DNA sequences were 5'-AAG CTG ACT CT-3' (11-mer), 5'-CAA GCT GAC TCT G-3' (13-mer), and 5'-ACA AGC TGA CTC TGC-3' (15-mer). Mismatched DNA sequences were 5'-AAG CTA ACT CT-3' (11-mer), 5'-CAA GCT AAC TCT G-3' (13-mer), and 5'-ACA AGC TAA CTC TGC-3' (15-mer).

Biotinamino-capronacid-amidodioctylmercaptopropionamide was synthesized in our laboratory.^{35,36} 11-Mercapto-1-undecanol, sodium chloride, monosodium phosphate (NaH₂PO₄), disodium phosphate (Na₂HPO₄), and absolute ethanol were purchased from Aldrich. The chemical structures and the sequences of the oligonucleotides used are summarized in Table I. Streptavidin was purchased from Kem-En-Tec Diagnostics. Water was purified using an ion exchange purification train (MilliQ system, Millipore).

TABLE I. Chemical structures of the thiols and the base sequences of the PNA probes and DNA targets used in this study. The underlined base A replacing a G in the middle of the DNA target sequence is the mismatching base to the PNA probe.

Mixed thiols	Biotinylated thiol	
	Spacer thiol	
PNA Probes	P- 11: Biotin- AEEA- AEEA-	AGAGTCAGCTT - NH2
	P- 13: Biotin- AEEA- AEEA-	CAGAGTCAGCTTG - NH2
	P- 15: Biotin- AEEA- AEEA-	GCAGAGTCAGCTTGT - NH2
*AEEA = 2-(2-aminoethoxy)ethoxyacetic acid		
DNA Targets	T- 11:	Cy5- 5'- AAGCTGACTCT - 3'
	T- mis- 11:	Cy5- 5'- AAGCT <u>A</u> ACTCT - 3'
	T- 13:	Cy5- 5'- CAAGCTGACTCTG - 3'
	T- mis- 13:	Cy5- 5'- CAAGCT <u>A</u> ACTCTG - 3'
	T- 15:	Cy5- 5'- ACAAGCTGACTCTGC - 3'
	T- mis- 15:	Cy5- 5'- ACAAGCT <u>A</u> ACTCTGC - 3'

B. PNA synthesis

PNA model sequences synthesized in this work were biotin-spacer-spacer-AGA GTC AGC TT-NH₂ (11-mer), biotin-spacer-spacer-CAG AGT CAG CTT G-NH₂ (13-mer), and biotin-spacer-spacer-GCA GAG TCA GCT TGT-NH₂ (15-mer). All PNAs were synthesized with a biotin group at the amino terminus, in order to be used for the sensor matrix assembling, separated by the main sequence by two aminoethoxy-ethoxy-acetyl groups (spacer). All PNAs were synthesized by solid phase methodologies by using an ABI 433A PNA synthesizer (Applied Biosystems) following the standard procedures indicated by the company, purified by semipreparative HPLC (C18 column, 250 × 10 mm²; flow, 4 ml/min; and gradient elution from H₂O+0.1% CF₃COOH to H₂O:CH₃CN 3:2+0.1% CF₃COOH), and characterized by ESI-MS (positive ions). Average yield after HPLC purification was 25%. Biotin-spacer-spacer-AGAGTCAGCTT-NH₂: calculated m/z , 884.6 (MH₄⁺), 707.9 (MH₅⁺), and 590.1 (MH₆⁺); found m/z , 884.2, 707.5, and 589.6. Biotin-spacer-spacer-CAGAGTCAGCTTG-NH₂: calculated m/z , 1020.2 (MH₄⁺), 816.3 (MH₅⁺), and 680.4 (MH₆⁺); found m/z , 1020.2, 816.5, and 680.6. Biotin-spacer-spacer-GCAGAGTCAGCTTGT-NH₂: calculated m/z , 1159.5 (MH₄⁺), 927.8 (MH₅⁺), and 773.3 (MH₆⁺); found m/z , 1158.6, 927.6, and 773.0.

C. Preparation of the sensor matrix

Figure 1 gives the schematics of the multilayer architecture of the sensor matrix. Cleaned glass substrates (LaSFN9, $n=1.85$ at 633 nm, Schott) were gold coated (~50 nm) by thermal evaporation ($p < 10^{-6}$ mbar, Edwards) and incubated overnight in a binary mixed solution of the biotinylated thiol and the spacer thiol (11-mercapto-1-undecanol) at a molar ratio of 1:9 and a total concentration of 0.5 mM in absolute ethanol.³⁷ After drying the substrates, an aqueous streptavidin (1 μM) solution was injected into the flow cell system in order to allow for binding to the mixed self-assembled thiol

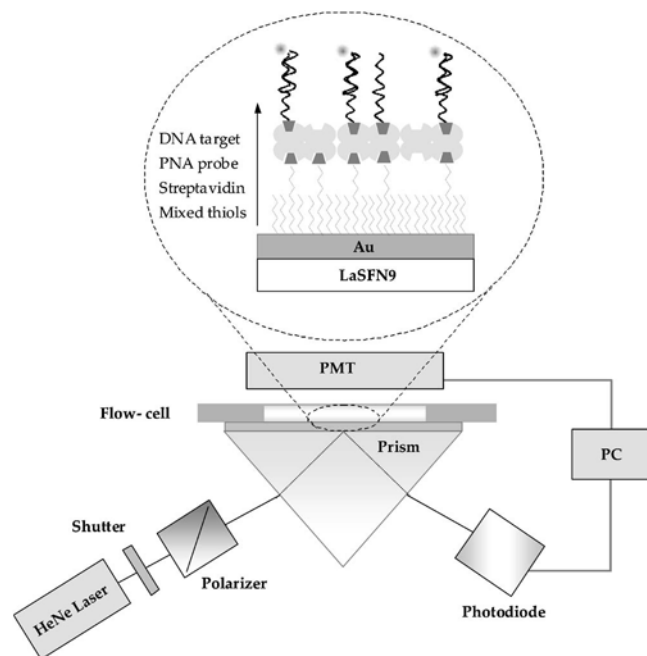


FIG. 1. Schematic drawing of the SPFS setup and the architecture of the sensor surface. A surface plasmon mode generated in the Kretschmann geometry was used to excite chromophore-labeled DNA targets interacting with PNA probes immobilized on a streptavidin layer. The fluorescence intensity is monitored in real time during hybridization.

layer at a flow rate of $10 \mu\text{l/s}$. Subsequently, biotinylated PNAs (500 nM in 10 mM phosphate buffer) as catcher probes were immobilized on the streptavidin layer.

D. Surface plasmon field-enhanced fluorescence spectroscopy (SPFS) measurement

The SPFS setup was constructed based on a conventional surface plasmon spectrometer in combination with a photon counting module.³⁸ A *p*-polarized HeNe laser beam (5 mW, $\lambda=632.8$ nm, Uniphase) was used to excite the surface plasmon waves. The incident laser is reflected off the base of the coupling prism (90° , LaSFN9, Schott), and the reflected intensity is focused by a lens ($f=50$ mm, Owis) for detection by a photodiode. The sample is mounted onto a two-stage goniometer (Huber) that can be rotated in $\Delta\theta=0.001^\circ$ steps. The emitted fluorescence light from the sample surface was collected through an interference filter ($\lambda=670$ nm, LOT) by a photomultiplier tube (Hamamatsu), which is mounted toward the back side of the sample (Fig. 1). The exposure time was controlled by placing a shutter in front of the sample, thus minimizing any photobleaching of the fluorescent dyes. Typically, the shutter was open for 5 s and closed for 3 min.

Kinetic measurements were performed by setting the angle of incidence at $\theta=55.5^\circ$. Kinetic curves were recorded as a function of time in both the reflectivity and fluorescence modes. All the kinetic experiments were performed with 1 ml for each target concentration at a flow rate of $10 \mu\text{l/s}$ using the same flow cell with an inlet and outlet and a closed loop circulation at room temperature ($T=24\pm 1^\circ\text{C}$). The buffer solutions were prepared in 10 mM phosphate, *p*H

$=7.4$, by adding sodium chloride (NaCl=20 and 137 mM, respectively). For a particular set of experiments, pure phosphate buffer solutions (without adding sodium chloride) were prepared at concentrations from 1 mM to 1M.

For the global analysis mostly employed in this study, Cy-5 labeled DNA target solutions (varying in concentration from 1 up to 200 nM) were introduced into the flow cell for the association phase, interacting with the PNA functionalized sensor surface for 10 min. After that the dissociation process was followed by rinsing with fresh buffer solution for each sample, also for 10 min. The surfaces could be fully regenerated by a short treatment with 10 mM NaOH, thereby removing all remaining bound target DNA for another analysis cycle on the same sensor surface.

E. Kinetic analysis of binding data

If the solution of a short oligonucleotide target is applied to a probe-modified sensor surface, it is difficult to observe a response with a good signal-to-noise ratio by SPR because the duplex formation with oligomeric DNA does not generate a significant change in the optical thickness. However, SPFS measurements demonstrated a high sensitivity for monitoring binding events between immobilized PNA and chromophore-labeled target DNA even at concentrations in the 100 fm (10^{-15}M) range.²⁰ This fluorescence intensity carries kinetic information of the hybridization process and can be analyzed in terms of the corresponding rate constants for association (k_{on}), dissociation (k_{off}), and the affinity constant (K_A).

The evaluation of the rate constants was performed by fitting the binding data using the 1:1 Langmuir model.^{39,40} All kinetic data were taken at different concentrations of the target DNA with PNA probes in two different ionic strength buffer solutions on the same sensor surface. Starting for a short period of time with a base line measurement [the intensity of the base line gives I_0 in Eq. (1)], solutions of varying concentrations of DNA targets were injected and circulated for approximately 10 min for the association process seen by the increasing fluorescence intensity. Then the cell was rinsed with fresh buffer solution for the dissociation process, again for 10 min.

Based on the Langmuir model the increase of the fluorescence intensity as a function of time is described by a simple bimolecular reaction,

$$I_{\text{fl}}(t) = (I_{\text{max}} - I_0)(1 - \exp(-k_a t)), \quad (1)$$

with

$$k_a = k_{\text{on}}c_0 + k_{\text{off}}, \quad (2)$$

and I_{max} being the maximum fluorescence intensity originating from surface bound targets at the given bulk concentration c_0 . I_0 is the initial background fluorescence.

The association kinetics is quantified with respect to the concentration dependence. Fitting the association phase data recorded from the injection of target to the rinsing step with

pure buffer with Eq. (1), the rate constant $k_a = k_{on}c_0 + k_{off}$ was obtained at each target concentration. The time-dependent dissociation is described by

$$I_{fl}(t) = (I_{max} - I_0)\exp(-k_{off}t). \quad (3)$$

The affinity constant (K_A) was obtained from the ratio of the rate constants, $K_A = k_{on}/k_{off}$. For each set of hybridizations, a series of 12 independent experiments was performed covering a range of target concentrations from 1 to 200 nM.

F. Melting temperature measurements

Stock solutions of PNA and DNA in distilled water were prepared, and their concentrations were measured by absorbance using the following ϵ_{260} ($M^{-1} \text{ cm}^{-1}$) for the nucleobases: T: 8800; C: 7300; A: 10 400; and G: 11 700.⁴¹ Each sample containing a PNA:DNA antiparallel couple was first incubated at 90 °C for 5 min and then slowly cooled to room temperature. All hybridization experiments were carried out using samples at a 5 μM concentration of each strand. Experiments at low ionic strength were done in a 10 mM phosphate buffer, 20 mM NaCl, and 0.1 mM ethylenediamine tetra-acetic acid (EDTA), pH 7.4. Experiments at high ionic strength were done in a 10 mM phosphate buffer, 137 mM NaCl, 2.7 mM KCl, and 0.1 mM EDTA, pH 7.4. Melting curves were recorded on a Perkin-Elmer BIO 20 spectrophotometer, equipped with a PTP 6 Peltier temperature programmer and a cell changer (Perkin-Elmer, Norwalk, CT). The samples were heated (1 °C/min, 5 points/min), and the absorbance at 260 nm was recorded. Melting temperatures were taken as the maximum of the first derivative of the melting curves. ΔH° and ΔS° of the hybridization reaction were obtained by a Van't Hoff fitting of the melting curves.⁴²

III. RESULTS AND DISCUSSION

Figure 1 shows the supramolecular architecture at the metal/solution interface composed of the mixed biotinylated thiol SAM, a streptavidin monolayer, and the layer of probe PNA coupled to the streptavidin binding matrix via the specific recognition of its biotin moiety. In Table I the structure of the thiols, PNA probes, and DNA targets are reported. The assembly of each layer was characterized by SPR. The calculated thicknesses of the gold, the mixed thiol, and the streptavidin layers were $d=57.5$ nm ($\epsilon' + i\epsilon'' = -12.38 + i1.38$), 1.5 nm ($\epsilon' = 2.25$), and 3.3 ($\epsilon' = 2.1$), respectively. The immobilization process of three PNAs of different lengths was monitored by SPR individually, as shown in Fig. 2. The rapid increase of the reflected intensity by the introduction of a 0.5 μM solution of probe PNA indicates their fast binding to the streptavidin matrix (binding affinity for streptavidin/biotin, $K_A = 10^{14} M^{-1}$). The different probe lengths result in an increasing thickness of the PNA layers (assuming a dielectric constant $\epsilon' = 2.1$), from $d=0.6$ nm for the 11-mer to 0.9 nm for the 13-mer and 1.3 nm for the 15-mer strand, respectively. This sensor architecture ensures a moderate catcher probe density in the range of one probe

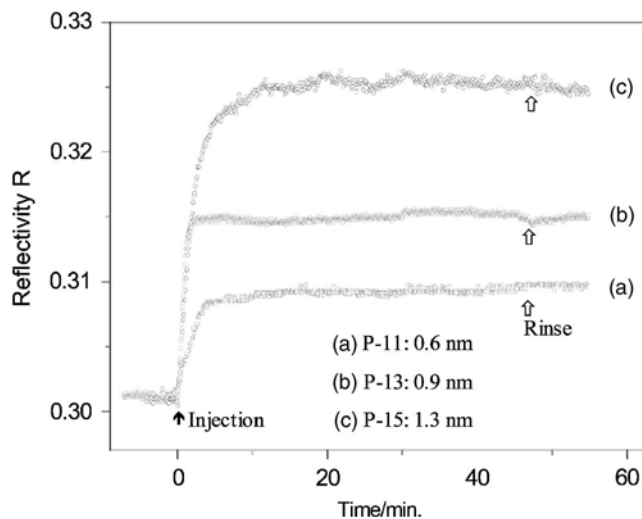


Fig. 2. Kinetic curves taken during the immobilization of three different PNAs after the injection (black arrow) of biotinylated PNAs in phosphate buffer solution. After a stable level of bound PNA was reached, the pure buffer solution was applied into the flow cell for rinsing. The calculated thicknesses for the PNA 11-mer (a), 13-mer (b), and 15-mer (c) were $d = 0.6, 0.9,$ and 1.3 nm, respectively.

per 40 nm² (2.5×10^{12} probes/cm²) minimizing any potential cross-talk between neighboring catcher probes and their target DNA during hybridization.

A. Influence of the ionic strength on the PNA/DNA hybridization in solution

In early works on PNA,²⁹ and in a previous systematic work,⁴³ the effect of ionic strength in full matched PNA:DNA duplexes in solution was analyzed. The stabilities of the PNA:DNA duplexes have a dependence on ionic strength different from that of DNA:DNA, since the former is slightly destabilized, while the latter is strongly stabilized by increasing the salt concentration.

In order to compare data obtained on the sensor surface with the behavior of the same sequences in solution, we analyzed the thermodynamic data of PNA:DNA interactions not only as a function of PNA length and of the ionic strength but also evaluated these in terms of mismatch recognition.

The thermodynamic data obtained in solution for the three PNAs of different lengths hybridized to MM0 (full match) and MM1 (single point mismatch) DNA target sequences at low and high ionic strengths are reported in Table II, together with the determined T_m 's. The data obtained for the full matched duplexes are consistent with those previously reported for PNA:DNA duplexes.^{29,43}

In all cases the melting temperatures increase with the PNA length, as expected by the higher number of base pairing, in good agreement with a statistical model proposed for the prediction of PNA:DNA melting temperatures.⁴⁴ The enthalpy gain and the entropy loss due to hybridization increase (in absolute values) with the length of the PNA and DNA sequences, consistent with the formation of more hydrogen bonds which leads to more stable duplexes and, at the same time, to higher losses of the degrees of freedom.

TABLE II. Enthalpy and entropy of the PNA/MM0 and PNA/MM1 DNA hybridization calculated at high and low ionic strengths in solution by a Van't Hoff fitting of the melting curves and melting temperatures obtained as maximum of the first derivative of the melting curves. The fitting of the melting curves of the 13-mer PNA with the MM1 DNA, both at high and low ionic strengths, resulted in large deviations from the actual curves, generating large errors (>30%) in the determination of the thermodynamic constants.

	ΔH° (kJ/mol) (\pm s.d.)	ΔS° (kJ/K mol) (\pm s.d.)	T_m ($^\circ$ C) (\pm s.d.)
High ionic strength MM0			
11-mer	-289 (\pm 20)	-0.75 (\pm 0.05)	64 (\pm 1)
13-mer	-330 (\pm 43)	-0.87 (\pm 0.11)	68 (\pm 1)
15-mer	-398 (\pm 20)	-1.04 (\pm 0.05)	75 (\pm 1)
High ionic strength MM1			
11-mer	-250 (\pm 40)	-0.68 (\pm 0.11)	43 (\pm 1)
13-mer	n.s.	n.s.	n.s.
15-mer	-306 (\pm 49)	-0.81 (\pm 0.13)	60 (\pm 1)
Low ionic strength MM0			
11-mer	-346 (\pm 17)	-0.91 (\pm 0.05)	68 (\pm 1)
13-mer	-398 (\pm 12)	-1.05 (\pm 0.03)	72 (\pm 1)
15-mer	-472 (\pm 24)	-1.24 (\pm 0.06)	77 (\pm 1)
Low ionic strength MM1			
11-mer	-270 (\pm 22)	-0.75 (\pm 0.06)	44 (\pm 1)
13-mer	n.s.	n.s.	n.s.
15-mer	-350 (\pm 21)	-0.94 (\pm 0.06)	61 (\pm 1)

Full matched PNA/DNA duplexes appear to be significantly more stable in low ionic strength media, an effect that was attributed to the polyelectrolyte behavior of the PNA:DNA duplex, with release of counterions upon complexation.⁴³ This effect is much less evident in the mismatched PNA/DNA duplexes, whose stabilities at high and low ionic strength are more similar. It may be reasoned that the presence of a mismatched pair of nucleobases in the duplex destabilizes the overall structure, thus preventing the strengthening of the helix at low ionic strength; in fact, the enthalpic increase from high to low ionic strength is around 20% for full matched structures, whereas it is only around 10% for mismatched structures. As a consequence of the different response to the environment polarity of fully matched and mismatched duplexes, mismatch recognition results are better in low ionic strength medium, as indicated by the differences in melting temperatures: it is evident that the best mismatch recognition in solution, i.e., the best differences between MM0 and MM1 structure stabilities, occurs at low ionic strength.

As far as the length of the PNA probes is concerned for mismatch recognition, according to the melting temperatures, the best mismatch recognition is found with the shortest 11-mer PNA, with the T_m differences between the full matched and the mismatched duplexes at high and low ionic strengths of 21 and 24 $^\circ$ C, respectively, whereas for the 15-mer PNA the corresponding figures are 15 and 16 $^\circ$ C.

Although the difference in enthalpy between the full matched and the mismatched structures is greater for the 15-mer than for the 11-mer, the entropic (unfavorable) contribution is also more pronounced for the former; therefore, due to a combination of these two effects, the shortest 11-mer PNA probe presents a better mismatch recognition in terms of T_m differences. Moreover, the T_m data parallel those obtained on the surface in terms of mismatch recognition as a function of length of the probe (see the following paragraphs). It has already been pointed out that the data on PNA/DNA hybridization obtained in solution give different stability constants and thermodynamic parameters than those obtained on a sensor surface,¹² although in the latter case data were previously obtained with SPR detection and therefore recorded with low sensitivity. It is interesting therefore to note the differences between the solution and the sensor surface using SPFS at low probe concentration, in order to better understand the specific effects of the hybridization process on sensor surfaces.

B. Influence of ionic strength of PNA/DNA duplex on the surface

The use of SPFS allows for the detection of the association of DNA on the PNA-modified surfaces at low target concentrations and at a definite (low) probe density, and therefore for the analysis of the effect of the bulk medium and of the probe size. Figure 3 shows various sets of hybridization data between MM0 DNA targets and surface attached PNA probes of different lengths at two different ionic strengths (NaCl=20 and 137 mM in 10 mM phosphate buffer solutions, respectively). For each kinetic measurement the association phase was recorded after the injection of target solutions, increasing the concentration of the targets from 1 to 200 nM after a short background measurement. The fluorescence intensity increased during hybridization. Then pure buffer was rinsed through the flow cell, thus initiating the dissociation process. The association rate increased with increasing concentration of the target DNA solution. By fitting each association phase using Eq. (1), an approximately linear relation of the measured rate constant k_a with target concentration c_0 was found. The association rate constant k_{on} is then obtained as the slope of the k_a vs c_0 plot [cf. Eq. (2)].

During the rinsing process, the dissociation is seen by the decreasing fluorescence intensity. As expected, the dissociation kinetics showed no significant dependence on the surface coverage. The dissociation rate constant was determined as the average k_{off} value obtained from fitting the dissociation phases using Eq. (3).

The collected results for the association and dissociation of PNA/DNA are given in Fig. 3 and Table III. One can see that there are no significant differences of the rate constants and the fluorescence intensities for each set of PNA/ DNA hybridization at both ionic strengths.

Similar sets of kinetic curves were obtained for one base mismatched DNA targets hybridizing to the PNA probes at the same sensor surface in two different buffer solutions, as shown in Fig. 4. The calculated rate constants are summa-

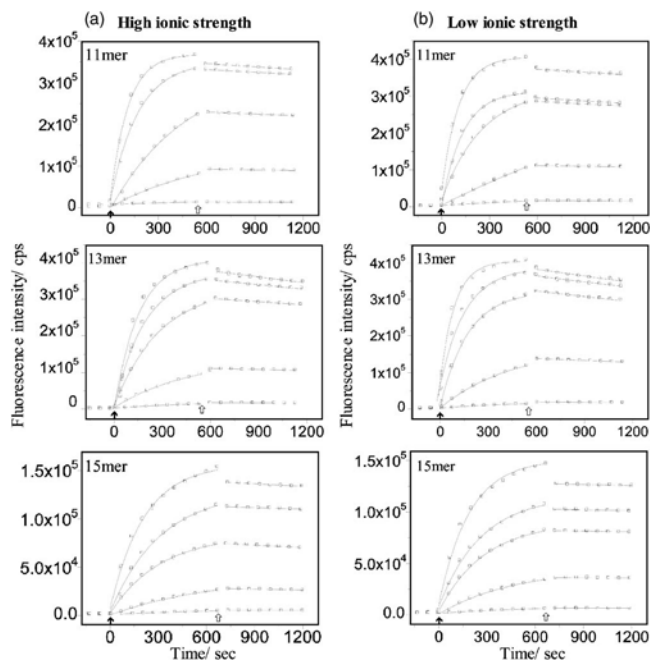


Fig. 3. SPFS measurements for the global analysis of the association and dissociation phases (taken at $\theta=55.7^\circ$). Open squares are data points collected every 1 min. The solid arrow (\uparrow) at $t=0$ indicates the injection of the target solutions of different concentrations for the recording of the association phase. The open arrows (\Downarrow) point to the beginning of the rinsing step for the dissociation phase. The solid lines are the best fit to a Langmuir model. Typical R^2 values after fitting are 0.999. The target concentrations are 1, 10, 50, 100, and 200 nM, respectively. (a) Hybridization between MM0 DNA targets and their PNA probes in high ionic strength buffer solutions. (b) Hybridization between MM0 DNA targets and their PNA probes in low ionic strength buffer solutions. The sensor surface was regenerated with 10 mM NaOH after rinsing for the next experiment.

ized in Table IV. The values of each set of PNA/DNA hybridizations at high and low ionic strength buffer solutions are virtually identical.

In order to investigate the lower limit of salt concentration for the MM0 11-mer PNA/DNA hybridization, seven different concentrations of the phosphate buffer solutions were prepared without adding additional salt. Figure 5 shows the experimental data for individual hybridization reactions of the MM0 DNA 11-mer targets (50 nM) to the surface attached PNA 11-mer probes at different ionic strengths. Once the hybridization reached equilibrium, the subsequent rinsing

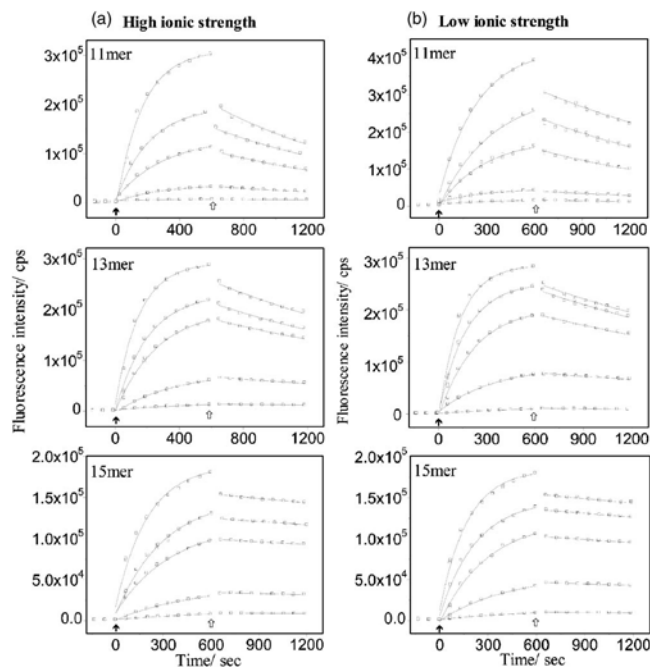


Fig. 4. SPFS measurements for the global analysis of the association and dissociation phases (taken at $\theta=55.7^\circ$). Open squares are data points collected every 1 min. The solid arrow (\uparrow) at $t=0$ indicates the injection of the target solutions of different concentrations for the recording of the association phase. The open arrows (\Downarrow) point to the beginning of the rinsing step for the dissociation phase. The solid lines are the best fit to a Langmuir model. Typical R^2 values after fitting are 0.999. The target concentrations are 1, 10, 50, 100, and 200 nM, respectively. (a) Hybridization between MM1 DNA targets and their PNA probes in high ionic strength buffer solution. (b) Hybridization between MM1 DNA targets and their PNA probes in low ionic strength buffer solution. The sensor surface was regenerated with 10 mM NaOH after rinsing for the next experiment.

step was monitored by changing to pure buffer solutions of the same ionic strength. Based on the Langmuir model, the rate constants k_{on} and k_{off} and the affinity constant K_A for the individual interactions were calculated and summarized in Table V.

DNA/DNA hybridization reactions, in general, are very ionic strength dependent. Various contributions to the observed effects have been identified: (1) first of all, DNA shows a limited solubility at low ionic strength; (2) at the single strand level, changing the ionic strength results in a change of the degree of stretching of these oligoelectrolytes;

TABLE III. Apparent kinetic rate constants and equilibrium constants for MM0 PNA/DNA hybridizations. The rate constants k_{on} and k_{off} and the affinity constant K_A were determined for each data set at different ionic strengths from the fit to a Langmuir model.

	High ionic strength			Low ionic strength		
	P-11/T-11	P-13/T-13	P-15/T-15	P-11/T-11	P-13/T-13	P-15/T-15
$k_{on}/(M^{-1} s^{-1})^a$	4.2×10^4	3.2×10^4	1.6×10^4	4.5×10^4	3.9×10^4	1.7×10^4
$k_{off}/(s^{-1})^a$	7.0×10^{-5}	4.1×10^{-5}	2.0×10^{-5}	7.6×10^{-5}	4.5×10^{-5}	2.0×10^{-5}
$K_A/(M^{-1})^b$	5.9×10^8	7.8×10^8	8.0×10^8	6.0×10^8	9.1×10^8	8.5×10^8

^aTypical R^2 after fitting for the k_{on} and k_{off} is above 0.999.

^b K_A values are calculated from k_{on} and k_{off} values.

TABLE IV. Apparent kinetic rate constants and equilibrium constants for MM1 PNA/DNA hybridizations. The rate constants k_{on} and k_{off} and the affinity constant K_A were determined for each data set at different ionic strengths from fits to the Langmuir model (cf. Fig. 4).

	High ionic strength			Low ionic strength		
	P-11/T-mis-11	P-13/T-mis-13	P-15/T-mis-15	P-11/T-mis-11	P-13/T-mis-13	P-15/T-mis-15
$k_{\text{on}}/(M^{-1} s^{-1})^a$	1.0×10^4	2.1×10^4	1.5×10^4	1.6×10^4	2.5×10^4	1.8×10^4
$k_{\text{off}}/(s^{-1})^a$	6.6×10^{-4}	4.5×10^{-4}	1.1×10^{-4}	7.9×10^{-4}	4.5×10^{-4}	1.3×10^{-4}
$K_A/(M^{-1})^b$	1.5×10^7	4.7×10^7	1.4×10^8	2.0×10^7	5.5×10^7	1.4×10^8

^aTypical R^2 after fitting for the k_{on} and k_{off} is above 0.999.

^b K_A values are calculated from k_{on} and k_{off} values.

(3) the hybridization reaction at a single site on the sensor surface strongly responds to any change in ionic strength of the bulk solution simply because the charges along the probes repel the cocharges along the target strands that are approaching from solution in low ionic strength buffer much more than at high ionic strength; and (4) single or double strands on individual sites on the sensor surface talk to their

neighbors via their electrostatic interaction unless they are sufficiently (laterally) separated. For the employed PNA catcher probe matrix only at the very beginning of the hybridization reaction, i.e., at a negligible DNA target surface coverage, the ionic strength does not play a role for the hybridization reaction. As soon as a significant fraction of the probe binding sites are occupied electrostatic cross-talk sets in. This can be clearly identified in Fig. 5 by at least two observations for the experiments in very low ionic strength buffer, the level of fluorescence intensity that is reached at saturation constantly increased with increasing ionic strength up to 10 mM. We interpret this dependence as a direct consequence of the electrostatic repulsion between neighboring DNA (target) strands leading to an effective reduction of the affinity constant and, hence, a reduced coverage for the lower ionic strength buffers at otherwise identical conditions, in particular, at identical bulk target concentrations. Nevertheless, it is remarkable that a significant hybridization could be observed even in pure water. This is impossible for DNA/DNA hybridization experiments given the solubility limits for DNA

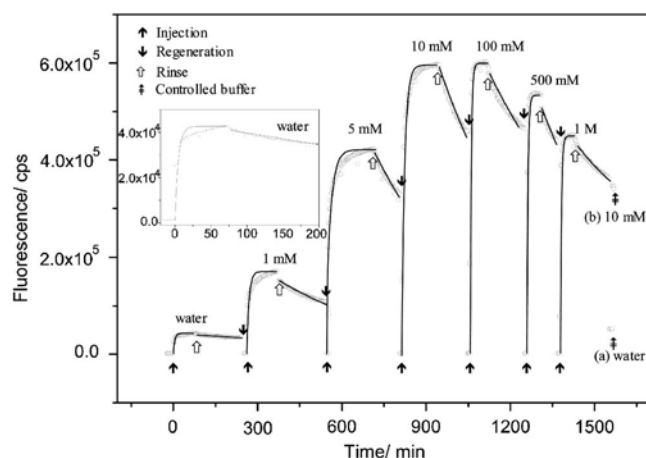


FIG. 5. Hybridization kinetics between a PNA 11-mer probe (P-11) and a DNA 11-mer target (T-11) at seven different phosphate buffer solutions. Kinetic curves were recorded by SPFS as a function of time (open circle). The solid arrows (↑) indicate the injections of the target DNA (50 nM) for the k_{on} determination, and the open arrows (⇑) indicate the rinsing with fresh buffer solution for the k_{off} determination. The sensor surface was regenerated (↓) with 10 mM NaOH for the next experiment. After the kinetic experiment in 1M phosphate buffer, the solution was exchanged (⇑) against pure water (a) and 1M (b). For the analysis of the rate constants for the PNA/DNA hybridization in different buffer solutions, the kinetic data were fitted by a Langmuir model. The inset shows the hybridization in water.

Other clear indications for an ionic strength dependent cross-talk between individual sites are the deviations in the kinetics with increasing coverage, again much more pronounced for the low ionic strength, e.g., 1 and 5 mM, than at high ionic strength, e.g., for a 1M buffer (cf. Fig. 5 and Table V).

Due to these deviations in the Langmuir fits, the obtained rate constants are only approximate. Nevertheless, it can be clearly seen that the ionic strength effect for PNA/DNA interactions does not result in any drastic changes of the rate

TABLE V. Rate constants and affinity constant for PNA 11-mer (P-11) and DNA 11-mer (T-11) hybridizations in different phosphate buffer solutions.

Buffer concentration c_0 (mM)	Hybridizations for P-11/T-11					
	1	5	10	100	500	1000
$k_{\text{on}}/(M^{-1} s^{-1})^a$	4.4×10^4	4.1×10^4	4.2×10^4	4.8×10^4	5.1×10^4	5.5×10^4
$k_{\text{off}}/(s^{-1})^a$	4.0×10^{-5}	4.8×10^{-5}	5.8×10^{-5}	5.9×10^{-5}	6.0×10^{-5}	5.6×10^{-5}
$K_A/(M^{-1})^b$	1.1×10^9	8.5×10^8	7.2×10^8	8.1×10^8	8.5×10^8	9.8×10^8

^aTypical R^2 after fitting for the k_{on} and k_{off} is above 0.999.

^b K_A values are calculated from k_{on} and k_{off} values.

constants compared with the situation for DNA/DNA hybridization.¹⁶ Because of the neutral nature of the PNA, the charge density accumulating at the interface during the hybridization with DNA is considerably lower than that of DNA/DNA hybridization reducing repulsion effects. Moreover, the increased stability of PNA/DNA duplexes at low ionic strengths observed in solution experiments is likely to play a role also in these surface experiments by counteracting the decreased stability due to DNA strand cross-talk.

For the hybridization in 10 mM phosphate buffer solution (NaCl=0 mM), the affinity constant was determined to be $K_A=7.2 \times 10^8 M^{-1}$. This is comparable to the values obtained in the 10 mM phosphate buffer solutions upon adding 20 mM ($K_A=6.0 \times 10^8 M^{-1}$) and 137 mM ($K_A=5.9 \times 10^8 M^{-1}$) NaCl presented in Fig. 3 and Table III. Indeed, the ionic strength shows little influence on the PNA/DNA hybridization kinetics, which is a good indication that, as compared to the solution experiments, a strong destabilizing factor is definitely playing a role. All these data collectively suggest that DNA interstrand cross-talk plays a strong role in lowering PNA/DNA affinity in surface systems.

For higher ionic strengths the fluorescence intensity decreases again. This phenomenon can be understood given the specifics of surface plasmon fluorescence optics: the chromophores near the metal/solution interface are excited by the evanescent field generated by the surface plasmon mode. The emitted fluorescence photons are monitored during hybridization in real time. In order to achieve an optimized fluorescence signal and not to decrease too much intensity by energy transfer to the metal substrate, the chromophores have to be separated sufficiently from the metal surface. If they are too close, they are quenched leading to a reduced fluorescence yield. The PNA/DNA duplexes at high ionic strength (500 mM and 1M) exhibit a more coiled configuration due to the strong screening of the target backbone charges by the counterions in solutions. As a result, the chromophores are closer to the metal surface losing fluorescence intensity. SPFS provides sufficient sensitivity for small changes in the configuration of PNA/DNA duplexes on a sensor surface.

C. Detection of point mutations on the surface

In order to demonstrate the potential of PNA probes in conjunction with the SPFS technique to detect point mutations, one base mismatched DNA target solutions were introduced into the flow cell and allowed to interact with the PNA probes at two different ionic strengths (NaCl=20 and 137 mM in 10 mM phosphate buffer solution). Figure 4 shows the kinetic curves for the 11-mer, the 13-mer, and the 15-mer PNA/DNA hybridizations, respectively. Following a short background measurement, the association phase was monitored after the injection of the 1 nM target solution, followed by the pure buffer rinse for the measurements of the dissociation kinetics. The hybridization experiments were carried out at varying target concentrations from 1 to 200 nM. The analysis of this experiment was also based on the Langmuir model. By fitting of each association phase

using Eq. (1), again an approximately linear relation between the measured rate constants and the bulk target concentration was found. The association constant k_{on} is obtained as the slope of a k_a versus concentration plot, and the dissociation constant was determined as the average of k_{off} values at the different concentrations. The collected results for the MM1 hybridization of PNA/DNA on the sensor surface are presented in Fig. 4 and Table IV.

The association rate constant is considerably slower than that of the fully complementary hybrid at both low and high ionic strengths, for all three lengths of PNA/DNA duplexes. In addition, the dissociation rate is much faster compared to the fully matched duplex. As a consequence, the affinity constant of the MM1 case is considerably lower than that of MM0. This indicates that excellent discrimination is possible for a point mutation using this PNA sensor matrix. Especially in the case of the 11-mer, the difference in the affinity constant between the MM0 and the MM1 duplexes is as large as a factor of 40. The fact that the shortest PNA probe performs the best mismatch recognition is perfectly consistent with what has been observed in solution experiments.

D. Probe length effect on the hybridization reaction

Three different lengths of oligonucleotides (11-mer, 13-mer, and 15-mer, respectively) were employed in order to investigate the probe length dependence for the PNA/DNA hybridization kinetics (for MM0 and MM1, and in two buffer solutions of different ionic strength) on the sensor surface and in solution. The 13-mer and 15-mer PNA samples have additional bases at each end of the PNA 11-mer (cf. Table I). For the MM0 case, the association rate constant of the 11-mer PNA/DNA hybridization was faster than that of the 13-mer and that of the 15-mer, as shown in Fig. 3 and summarized in Table III. Once the PNA/DNA hybrid is formed, the 15-mer duplex having four more base pairs is more stable than the 11-mer. This tendency of the length effect for the PNA/DNA hybridization is also consistent with what has been observed in solution, thus pointing out that the same enthalpic gain, due to the formation of more hydrogen bonds, is also prevailing on the sensor surface.

Thus, the dissociation rate constant of the long PNA/DNA is much slower than that of the short one. Consequently, the affinity constant of the 15-mer PNA/DNA is slightly higher than those of the 13-mer and the 11-mer; however, the length dependence for the MM0 situation is not so pronounced.

The hybridization for the MM1 case depends much more on the probe and target length, as shown in Fig. 4 and summarized in Table IV. The dissociation rate for the 11-mer was much faster than that of the 13-mer and the 15-mer. The one base mismatched duplex is substantially less stable than the fully matched duplex (a factor of 40 difference of the affinity constant for the 11-mer). However, the difference of the affinities between the MM0 and the MM1 cases for the 13-mer and for the 15-mer is only a factor of 10, again paralleling what was observed with T_m measurements in solution.

IV. CONCLUSIONS

The present study has clearly demonstrated the influence of the ionic strength for PNA/DNA hybridization on the well-established sensor surface employing self-assembly strategy and in the solution. SPFS provides enough sensitivity for kinetic analysis in real time as well as small configurational change of PNA/DNA duplex on the sensor surface.

Indeed, although low ionic strength definitely favors PNA/DNA hybridization in solution, it does not play a dominant role on PNA/DNA hybridization kinetics on the sensor surface, likely due to the opposite destabilizing effect of interstrand DNA cross-talk, which is strongly enhanced at low salt concentrations. However, the fluorescence intensity could be affected according to the change of distance between surface and PNA/DNA duplex generated by the ionic strength. The limit of ionic strength for detection of DNA target was qualified by varying the concentration of ionic strength from water to 1M phosphate buffer solution with providing maximum fluorescence window (10–100 mM). The discrimination between fully matched and single base mismatched hybridizations on the sensor surface was accomplished with significant difference of the affinity constants. The best discrimination was achieved using the 11-mer PNA, while it was less effective for 13-mer and 15-mer. Thus, the design of PNA sensors targeted toward detection of point mutations should take into account this effect, with a balance between the need to increase the length in order to have gene specificity and that to decrease it in order to achieve the best mismatch recognition.

The major benefits of using PNA as a probe, i.e., overcoming the limits of ionic strength (even with hybridization in water) and efficiently detecting a point mutation, were demonstrated possible also on a sensor surface, showing that PNAs can be promising probes for the development of DNA sensors.

ACKNOWLEDGMENTS

This work was partially supported by the European Union (Project No. QLK1-2000-31658, "DNA-Track") and by the Deutsche Forschungsgemeinschaft (KN 224/13-1).

- ¹D. R. Thévenot, K. Toth, R. A. Dust, and G. S. Wilson, *Pure Appl. Chem.* **71**, 2333 (1999).
- ²S. Löfås, M. Malmqvist, I. Rönnberg, E. Stenberg, B. Liedberg, and I. Lundström, *Sens. Actuators B* **5**, 79 (1991).
- ³R. Cush, J. M. Cronin, W. J. Steward, C. H. Maule, J. Molloy, and N. J. Goddard, *Biosens. Bioelectron.* **8**, 347 (1993).
- ⁴A. Bernard and H. R. Bosshard, *Eur. J. Biochem.* **230**, 416 (1995).
- ⁵D. J. van den Heuvel, R. P. Kooyman, H. J. W. Drijfhout, and G. W. Welling, *Anal. Biochem.* **215**, 223 (1993).
- ⁶P. Schuck, *Annu. Rev. Biophys. Biomol. Struct.* **26**, 541 (1997).
- ⁷J. H. Lakey and E. M. Raggett, *Curr. Opin. Struct. Biol.* **8**, 119 (1998).
- ⁸S. J. Wood, *Microchem. J.* **47**, 330 (1993).
- ⁹P. Nilsson, B. Persson, M. Uhlen, and P. A. Nygren, *Anal. Biochem.* **224**, 400 (1995).

- ¹⁰M. Gotoh, Y. Hasegawa, Y. Shinohara, M. Shimizu, and M. Tosu, *DNA Res.* **2**, 285 (1995).
- ¹¹T. Herne and M. Tarlov, *J. Am. Chem. Soc.* **119**, 8916 (1997).
- ¹²K. K. Jensen, H. Ørum, P. E. Nielsen, and B. Norden, *Biochemistry* **36**, 5072 (1997).
- ¹³E. Kai, S. Sawata, K. Ikebukuro, T. Iida, T. Houda, and I. Karube, *Anal. Chem.* **71**, 796 (1999).
- ¹⁴D. Piscevic, R. Lawall, M. Veith, M. Liley, Y. Okahata, and W. Knoll, *Appl. Surf. Sci.* **90**, 425 (1995).
- ¹⁵T. Liebermann and W. Knoll, *Colloids Surf., A* **171**, 115 (2000).
- ¹⁶T. Neumann, M.-L. Johansson, D. Kambhampati, and W. Knoll, *Adv. Funct. Mater.* **12**, 575 (2002).
- ¹⁷W. Knoll, M. Liley, D. Piscevic, J. Spinke, and M.-J. Tarlov, *Adv. Biophys.* **34**, 231 (1996).
- ¹⁸D. Kambhampati, P.-E. Nielsen, and W. Knoll, *Biosens. Bioelectron.* **16**, 1109 (2001).
- ¹⁹W. Knoll, H. Park, E.-K. Sinner, D. Yao, and F. Yu, *Surf. Sci.* **570**, 30 (2004).
- ²⁰D. Yao, F. Yu, J. Kim, J. Scholz, P. Nielsen, E. K. Sinner, and W. Knoll, *Nucleic Acids Res.* **32**, 177 (2004).
- ²¹P.-E. Nielsen, M. Egholm, R.-H. Berg, and O. Buchardt, *Science* **254**, 1497 (1991).
- ²²J. Anastassopoulou, *J. Mol. Struct.* **651**, 19 (2003).
- ²³N. M. Luscombe, R. A. Laskowski, and J. M. Thornton, *Nucleic Acids Res.* **29**, 2860 (2001).
- ²⁴A. K. Todd, A. Adams, J. H. Thorpe, W. A. Denny, L. P. Wakelin, and C. J. Cardin, *J. Med. Chem.* **25**, 536 (1999).
- ²⁵J. Liu, L. Malinina, T. Huynh-Dinh, and J. A. Subirana, *FEBS Lett.* **438**, 211 (1998).
- ²⁶Y. Gao, M. Sriram, and A. H.-J. Wang, *Nucleic Acids Res.* **21**, 4093 (1993).
- ²⁷L. Rulisek and Z. Havlas, *J. Am. Chem. Soc.* **122**, 10428 (2000).
- ²⁸V. Tereshko, C. J. Wilds, G. Minasov, T. P. Prakash, M. A. Maier, A. Howard, Z. Wawrzak, M. Manoharan, and M. Egli, *Nucleic Acids Res.* **29**, 1208 (2001).
- ²⁹M. Egholm, O. Buchardt, and L. E. A. Christensen, *Nature (London)* **365**, 566 (1993).
- ³⁰P. E. Nielsen, *Curr. Opin. Biotechnol.* **10**, 71 (1999).
- ³¹A. Germini, A. Mezzelani, F. Lesignoli, R. Corradini, R. Marchelli, R. Bordoni, C. Consolandi, and G. De Bellis, *J. Agric. Food Chem.* **52**, 4535 (2004).
- ³²S. Sawata, E. Kai, K. Ikebukuro, T. Iida, T. Honda, and I. Karube, *Biosens. Bioelectron.* **14**, 397 (1999).
- ³³G. Feriotto, R. Corradini, S. Sforza, C. Mischianti, R. Marchelli, and R. Gambari, *Lab. Invest.* **81**, 1415 (2001).
- ³⁴R. Corradini, G. Feriotto, S. Sforza, R. Marchelli, and R. Gambari, *J. Mol. Recognit.* **17**, 76 (2004).
- ³⁵W. Knoll, F.-J. Schmitt, and C. H. Klein, *International Patent No. WO 92/10757* (1992).
- ³⁶J. Spinke, M. Liley, F. J. Schmitt, H. J. Guder, L. Angermaier, and W. Knoll, *J. Chem. Phys.* **99**, 7012 (1993).
- ³⁷J. Spinke, M. Liley, H. J. Guder, L. Angermaier, and W. Knoll, *Langmuir* **9**, 1821 (1993).
- ³⁸T. Liebermann, W. Knoll, P. Sluka, and R. Herrmann, *Colloids Surf., A* **169**, 337 (2000).
- ³⁹I. Langmuir, *J. Am. Chem. Soc.* **40**, 1361 (1918).
- ⁴⁰R. Karlsson, A. Michaelsson, and L. Mattsson, *J. Immunol. Methods* **145**, 229 (1991).
- ⁴¹S. Sforza, G. Haaima, R. Marchelli, and P. E. Nielsen, *Eur. J. Org. Chem.*, 197 (1999).
- ⁴²L. A. Marky and K. J. Breslauer, *Biopolymers* **26**, 1901 (1987).
- ⁴³S. Tomac, M. Sarkar, T. Ratilainen, P. Wittung, P. E. Nielsen, B. Nordén, and A. Graslund, *J. Am. Chem. Soc.* **118**, 5544 (1996).
- ⁴⁴U. Giesen, W. Kleider, C. Berding, A. Geiger, H. Orum, and P. E. Nielsen, *Nucleic Acids Res.* **2**, 5004 (1998).